Hydrodynamics, sediment transport and morphological features at the confluence between the Yangtze River and the Poyang Lake

Saiyu Yuan[1,2], Hongwu Tang[1,2*], Kun Li[1], Lei Xu[1], Yang Xiao[1,2], Carlo Gualtieri[3], Colin Rennie[4], Bruce Melville[5]

[1] State Key Laboratory of Hydrology-Water Resources and Hydraulic Engineering, Hohai University, Nanjing, China.

[2] Yangtze Institute for Conservation and Development, Nanjing, China.

[3] Department of Civil, Architectural and Environmental Engineering, University of Napoli Federico II, Naples, Italy.

[4] Department of Civil Engineering, University of Ottawa, Ottawa, Canada.

[5] Department of Civil and Environmental Engineering, University of Auckland, Auckland, New Zealand

Corresponding author: Professor Hongwu Tang (hwtang@hhu.edu.cn)

Key Points:

- Two field surveys on the river confluence of Yangtze River and the outflow channel of Poyang Lake were conducted.
- Flow structure, suspended sediment transport and morphology of this large river confluence have been studied.

This article has been accepted for publication and undergone full peer review but has not been through the copyediting, typesetting, pagination and proofreading process, which may lead to differences between this version and the Version of Record. Please cite this article as doi: 10.1029/2020WR028284.

- Large-size helical motions were observed that likely played important roles in suspended sediment transport and local morphology.

Abstract

Confluences act as critical nodes in a river network as they affect flow, sediment transport, water quality and ecological patterns. A complete knowledge about hydro-morpho-sedimentary processes at river confluences is still incompleted and it has been usually accepted that secondary flows are weak because of the significant role of form roughness in large rivers. In this study, two field surveys were conducted on the flow structure, suspended sediment transport and morphology of the confluence between the Yangtze River (the largest river in China) and the Poyang Lake (the largest freshwater lake in China). Dual counter-rotating cells were observed during high flow conditions and a single secondary cell appeared in low flow conditions. These helical cells restricted the core size of high sediment concentration and downwelling flows acted as a barrier hindering the exchange of sediment between the two rivers. Furthermore, the observed large scour hole was likely related to the downwelling and upwelling flows caused by helical motions. In low flow conditions the scour hole looked like a deep channel, which was likely related to a long-surviving helical cell. The scour hole disappeared further downstream, when either the helical motion got weak during low flow conditions, or when a reverse helical cell occurred during high flow conditions. Hydrodynamics, suspended sediment transport and morphological features observed at such a large confluence demonstrated that river planform geometry and discharge ratio affected the flow structure, especially the helical motion. This in turn affected sediment transport as well as the local bed morphology.

Key words:

River confluence; helical cells; bed morphology; sediment transport; Yangtze River; Poyang Lake

1 Introduction

Confluences are critical nodes in a river network and affect flow, sediment transport, water quality and ecological patterns. Significant changes in hydrodynamics, bed morphology as well as environmental and ecological features occur at the confluence, where the flows from two tributaries combine and adjust to the post-confluence planform geometry. Confluence of two flows with different momentum and velocity ratios (the ratio of the variable of one channel to that of the other) often results in a downstream shear layer driven by the Kelvin-Helmholtz (KH) instability. It enhances turbulent mixing and exchange of momentum and other matter (e.g., sediment and pollutants; Rhoads & Sukhodolov, 2001; Sukhodolov & Rhoads, 2001; Tang et al., 2018; Yuan et al., 2019) during the spatial growth of the vortex pairing (Winant and Browand, 1974). In-depth knowledge of the dynamics of confluences, especially for large rivers, is required to mitigate flooding, manage water resources and improve protection of the water environment and ecology. A large number of studies in literature have focused on small-scale channel confluences with small width-to-depth ratios (W/H <10) (e.g., Baranya et al., 2015; Riley & Rhoads, 2011). More recently, an increasing number of studies have been undertaken to study confluences at medium scale (10< W/H <50) (Ramón et al., 2013; Konsoer and Rhoads, 2014; Riley et al., 2014; Martín-Vide et al., 2015; Biron et al., 2019; Luz et al., 2020) and at large scale (W/H > 50) (Best and Ashworth, 1997; Parsons et al., 2007; Lane et al., 2008; Szupiany et al., 2009; Gualtieri et al., 2018; Ianniruberto et al., 2018). The main findings from studies on small, medium and large confluences are briefly reviewed.

Deflection of flow, flow stagnation upstream and near the confluent apex, flow separation from the wall as the tributary enters the confluence hydrodynamics zone (CHZ), the mixing interface between two confluent flows, helical motions caused by the curvature of the tributaries,

etc., have been well documented at small channel confluences (e.g., Best, 1987; Rhoads and Kenworthy, 1995, 1998; Bradbrook et al., 1998; Rhoads et al., 2009; Bradbrook et al., 2000). Different momentum and velocity ratios of the two confluent flows lead to interfaces having different mixing mechanisms. The shear layer characterized by von Kármán vortex street for the momentum ratios close to unity, i.e. wake mode (Constantinescu et al., 2011; Constantinescu et al., 2012) or vortex pairing for those far from unity, i.e. KH vortices dominating mode (Rhoads and Sukhodolov, 2004) were reported. However, based on drone imagery, Biron et al. (2019) observed that only KH vortices dominated within the shear layer for discharge ratios ranging from 0.09 to 1.02 in a medium-sized confluence. Twin surface-convergent helical cells were observed on either side of the shear layer in a vertical plane, which rapidly evolve into a single, channel-scale circulation cell due to the differences in the curvature of the two combining flows (Bradbrook et al., 2000; Rhoads & Kenworthy, 1995, 1998). Bed discordance (defined as the difference in bed elevation between two channels) can destroy the quasi two dimensionality of the mixing interface and result in distortion of the shear layer; consequently, upwelling of water can take place at the downstream junction corner (Biron et al., 1996a, 1996b; Bradbrook et al., 2001; De Serres et al., 1999), which affects sediment transport and bed morphology (Biron et al., 1993; Boyer et al., 2006; Sukhodolov et al., 2017). Moreover, the large lateral advection of the mean flow, associated with helical motions, can also result in the distortion of the shear layer (Rhoads & Sukhodolov, 2008; Yuan et al., 2016). Even differences in water density between two flows may impact the local hydrodynamics around the confluence (Rhoads and Kentworthy, 1998; Biron and Lane, 2008; Ramòn et al, 2013; Lyubimova et al., 2014; Cheng and Constantinescu, 2018; Gualtieri et al., 2019).

A mid-stream deep scour hole and bank-attached lateral bars, related to flow separation, are some of the principal morphological features identified at river confluences (Best, 1988). Field surveys (Biron et al., 1993; Boyer et al., 2006; Rhoads et al., 2009; Ianniruberto et al., 2018) and laboratory experiments (Best, 1988; Guillén-Ludeña et al., 2015, 2016; Guillén-Ludeña et al., 2017; Leite Ribeiro et al., 2012; Yuan et al., 2018; Yu et al., 2020) on sediment transport and morphology at channel confluences were conducted in the past to investigate the interaction between flow dynamics and the bed morphology. Many features, such as large flow velocity, strong turbulence, effects of the shear layer or curvature-induced helical circulations were believed to be the cause of the mid-stream scour hole formation. However, recently, Yuan et al. (2018) reported on the basis of flume experiments that downwelling and upwelling flows of helical motions, associated with the intense bed shear, are responsible for sediment entrainment and scouring. These flows produce and promote the mid-channel scour hole observed in flume experiments. Qualitative as well as quantitative observations suggest that sediment is transported essentially along the flanks of the scour hole, thereby the scour hole is maintained in a stable condition (Mosley, 1976; Best, 1988; Boyer et al., 2006). The limitations of almost all of these studies are that they were conducted in small river confluences or in laboratory flumes.

Parsons et al. (2007) highlighted some similarities between the flow and bed morphology of small and large confluences. Some differences were attributed to increase in ratio of width to depth for large-scale channels. They suggested an increase in the role of the form roughness and possible differences in the mechanisms generating secondary flows as the channel scale increases. Lane et al. (2008) reported that turbulent shear mixing, associated with a near-vertical shear layer occurred very close to the junction and the large-size secondary circulation was beneficial for the rapid mixing of two large confluent flows. Szupiany et al. (2009) conducted

field surveys on the dynamics of large braided-bar confluences in the Río Paraná and indicated that the scale might be an important factor governing the confluence dynamics. For large width-to-depth ratios it was suggested that the influence of secondary currents decreased because of an increase in the role of the form roughness. At the end, it is not straightforward to extend the current understanding of small confluences to large confluences. The knowledge of the hydro-morpho-sedimentary processes at river confluences is still incomplete, especially at the large ones.

The present study was undertaken to investigate hydrodynamics, sediment transport and morphological features at the large confluence between the Yangtze River and the outflow channel of Poyang Lake. They are the largest river and the largest freshwater lake in China, respectively. Both of them have dramatic influence on flood control, water resource management, and environmental and ecological protection for the Yangtze River basin. In that reach, Yangtze river has a width in the average of almost 2 km. The authors have attempted to address three aspects: (1) the existence and importance of helical cells at the confluence; (2) suspended sediment transport; (3) the bed morphological features related to hydrodynamics and sediment transport. The current results can assist in the protection of the local water body, as well as expand the present database and knowledge on the dynamics of large river confluences.

2 Study site, field procedures, and methods

2.1 Study site

The Yangtze River catchment is one of the largest drainage basins in the world, its annual water discharge (9000×10^8 m^3/yr) and sediment load (4.78×10^8 t/yr) are ranked as the fifth and fourth largest in the world, respectively. The Poyang Lake is located at the junction of the south

bank of the Yangtze River (Figure 1), with a basin area of 16.2×10^4 km^2 and accounts for 9% of the Yangtze River drainage area (Xu et al., 2001). The confluence is located in the middle and lower reaches of the Yangtze River, at about 900 km downstream of the Three Gorges Dam (detailed information about this dam can be found on Global Reservoir and Dam Database, Version 1.1; Lehner et al., 2011) and 800 km upstream of the river mouth. The confluence is formed as the only outflow channel of the Poyang Lake joins to the Yangtze River. It is a critical node that affects flood control, water resource and ecology of the Poyang Lake and is a prominent place for shipping in Jiangxi Province. When the water level in the Yangtze River is higher than that in the Poyang Lake during the flood season, part of the river flow enters into the Poyang Lake (i.e. backwater condition exists). The operation of the Three Gorges Dam, for which impoundment started in 2003, brought large benefits on flood control, navigation and electricity production, but affected fluvial, and environmental and ecological processes (e.g., its negative effects on the finless porpoises; Stone, 2008) downstream along the Yangtze River as well as its tributaries. The downstream water level has decreased by 3.9%-13.5% at 15 main gauging stations after the operation of the Three Gorges Dam, and such decrease is especially evident in the fall (Yang et al., 2006). Severe channel erosion has occurred, and the maximum erosion downstream of the dam can reach 10 m (Zheng et al., 2018). The dam operation can also partially explain the reduced sedimentation in the downstream-linked two largest Chinese freshwater lakes, Dongting Lake and Poyang Lake (Zhou et al., 2016). Previous studies have demonstrated that the operation of the Three Gorges Dam has weakened the backwater effects of the Yangtze River on the Poyang Lake, resulting in an advanced and lengthened dry season in the Lake (e.g., Guo et al., 2012). Therefore, a comprehensive study of this confluence will not

only advance our current knowledges about large river confluences but also will be useful for the better management of this critical river-lake system.

2.2 Instrumentation and field procedures

Two field surveys were carried out in 2018, first during high flow conditions (Survey 1; 10-14 August 2018) and later during low flow conditions (Survey 2; 8-12 December 2018). During each of the five-day survey measurements, water levels and flow discharges did not show any significant change (Figure 2). A large difference in water levels of about 5.8 m was observed between the two surveys. Large variation of water level led to submergence and emergence of large tracts of floodplain (occupying about half of the channel width) at the mouth of the Poyang Lake depending on the high or low flow conditions, respectively. The discharge of the Yangtze River in Survey 1 was twice larger than that in Survey 2, whereas the outflow of the Poyang Lake was similar in the two surveys (Table 1).

A large island, Zhangjia Island, bifurcates the Yangtze River at the Jiujiang Station, and the river merges again about 19 km downstream of Jiujiang Station with a confluence angle of nearly 90 degrees (Figure 1), i.e. the branch at the left of this island also belongs to the Yangtze River. For simplicity, the Yangtze River mentioned hereafter means the branch at the right of the Zhangjia Island. The mid-channel island, Guan Island, separates the flow of the Yangtze. The main stream lay on the left of the island, which had a discharge twice larger than that of the right branch in Survey 1. The two bifurcated channels converged at the end of the island with a confluence angle of about 20 degrees. The Meijia Island is located at the apex of the confluence of the Yangtze and the Poyang and has a confluence angle of about 58 degrees.

A total of 17 cross sections was used for the two tributaries and the post confluence for Survey 1 and 19 cross sections were used for Survey 2 (includes split cross section, CYP0, and an additional one, CYP8-A; Figure 1). Two acoustic Doppler current profilers (ADCPs), namely a Sontek River Surveyor M9 Instrument and a Rio Grande 600kHz RDI Instrument, were used simultaneously. The data obtained by the two devices were compared to assure their accuracy. The ADCPs provided three-dimensional flow velocities over the water depth along these cross-sections, backscatter intensity, which can be related to total suspended sediment concentration (TSS) after calibration, as well as bed elevations. All measurements were georeferenced using a differential global positioning system (DGPS). Since the ADCPs were deployed from a moving vessel, they were linked to the DGPS to provide both position and boat velocity. The compass was well calibrated, the boat velocity and track position of the survey lines were monitored online and were held constant as much as possible during the surveys. A steady boat velocity of 2 m/s was adopted to decrease the number of missing ensembles, as well as keep the boat movement in a relatively straight line. The vertical bin size of velocity measurement of RDI was fixed as 0.5 m, while the Sontek M9 firmware changes the acoustic operating frequency and thus depth measurement resolution depending on the water depth and velocity (Moradi et al., 2019).

For both ADCP M9 and ADCP RDI, the averaging interval (*AI*) used, herein, was 1 second. Considering the boat speed as 2.0 m/s, which was of the order of the flow velocity, the measured velocity represented the flow conditions of an average volume that is 2 m long near the water surface and the approximate value of water depth near the bed (about 30 m in maximum herein; Rennie et al., 2002). At the confluence, the channel widths varied between 1,000 m to 3,000 m, thus the assumption of flow homogeneity was properly satisfied for this scale (Szupiany et al., 2009). In order to obtain representative values of the time-averaged three-

dimensional velocities at each cross section, measurements along series of multiple repeated-transect lines (two repeats for Survey 1 for the sake of safety during the high flow conditions and four repeats for Survey 2) were conducted and averaged subsequently.

During both surveys, suspended sediment concentration was measured. A total of 17 vertical profiles in Survey 1 and 20 vertical profiles in Survey 2 were chosen for water sampling during the campaign. Depending on the water depth, 3~6 samples in one vertical were taken. Furthermore, the TSS concentration was measured by filtering, drying and weighing.

2.3 Data post-processing

RDI data and M9 data were exported as ASCII files and MATLAB files using Teledyne RDI WinRiverII software and RiverSurveyor Live software. The data for multiple transects were then analyzed using the Velocity Mapping Tool (VMT), a suite of MATLAB routines with a graphical user interface (Parsons et al., 2013). VMT composites and averages ADCP velocity data from repeat transects along cross-sections, providing the capability to plot 3-D velocity vectors. In this study, the average velocity data from M9 were processed to analyze the flow structure, and the data from RDI were used mainly to verify their accuracy. RDI data also provide the information about acoustic backscatter intensity.

A source of debate exists about the correct and robust definition of secondary currents within river channels (Lane et al., 1999, 2000; Rhoads and Kenworthy, 1999). Lane et al. (2000) summarized four current definitions for the secondary flows: (1) the centerline definition; (2) the Rozovskii definition; (3) the zero net cross-stream discharge definition; and (4) the discharge continuity definition. Constraints exist with the methods of data collection and rotation of secondary current vectors at the confluence of the Yangtze River and the Poyang Lake with very

large average channel widths. First, significant transverse variations in the main flow direction can often complicate identification of the primary flow direction and thus the definition of a robust frame of reference. Second, the location of a given reference section is particularly difficult to determine at confluences, since the primary flow changes its curvature permanently and is in opposite directions at both sides of the confluence mixing layer. These constraints result in the centerline definition and methods that define only one secondary plane across an entire section (i.e. the discharge continuity and the zero net cross-stream discharge procedures) for rotation of secondary velocities often being problematic to apply (Szupiany et al., 2009). The Rozovskii reference frame rotated each vertical ensemble of velocity measurements such that primary and secondary velocity components were aligned parallel and perpendicular to the orientation of the depth-averaged velocity vector, respectively. This was useful especially for identifying helical motion in strongly converging flows (Rozovskii, 1957; Rhoads and Kenworthy, 1998; Szupiany et al., 2009). However, Lane et al. (2000) noted that in the Rozovskii rotation the identification of helical circulation is inevitable. Therefore, the present study uses the Rozovskii definition calculated by VMT, and the raw data of some cross sections have also been given to relate the Rozovskii frame back to the channel frame.

Acoustic Doppler technology provided quantitative information on suspended sediment concentrations (Creed et al., 2001; Filizola and Guyot, 2004; Kostaschuk et al., 2005; Sontek, 1997) through an analysis of the backscatter intensity. This intensity is a function of both the equipment characteristics (frequency, transmitted power, measured volume range, received sensitivity) and the flow conditions (concentration and size of sediment particles, amount of organic matter, dissolved solids and air bubbles, (Sontek, 1997)). Therefore, for a given instrument, i.e. RDI ADCP herein, and for a constant sediment type and grain size distribution,

the signal strength can have a simple correlation with the sediment concentration in the absence of air bubbles and particulate organic matter. Baranya and Józsa (2013) proposed a method to define the relationship between suspended sediment concentration and the variable *RB* which is derived from the acoustic backscatter intensity. Past work has shown that using the information of the backscatter intensity signal of ADCPs is a useful method for characterizing spatial patterns of suspended sediment within confluences (Zinger et al., 2013; Konsoer and Rhoads, 2014; Rhoads and Johnson, 2018). Hence, patterns of *RB* were used here as a surrogate for suspended sediment concentration.

3 Results and discussion

3.1 Bed morphology variation related to operation of the Three Gorges Dam

Bed morphology of the confluence before the operation of the Three Gorges Dam in October 2001 (Figure 3a) and post-operation in October 2016 (Figure 3b), and in August and December of 2018 (Figure 3c-d), as well as some cross-sectional bed surface profiles (Figure 3e-g), were compared. The elevations are with reference to the frozen base level whose zero datum is 1.91 m higher than that of the 1985 National Height Datum. Comparison between 2001 (Figure 3a) and 2018 (Figure 3c) surveys, when the confluence had gone through a flood season, depicts a similar planform of the thalweg. However, the bed elevation of Yangtze River, especially at beginning of post-confluent reach in 2018 (Figure 3e and f) was about 5 m lower than that in 2001. This could be attributed largely to the decrease in sediment concentration in the Yangtze River due to the upstream dam. The effects were weakened significantly near CYP5 (Figure 1c). The thalweg of the Yangtze River in 2016 was even 5 m deeper than that in Survey 1 of 2018 and deviates to the left. This may be attributed to the large flood of 2016, which was

the largest since 1998. The bed morphology at the mouth of the outflow channel of Poyang Lake in the two plots look similar as they have been mainly controlled by the upstream flow and sediment fed by the Poyang Lake, which did not suffer radical changes. It could be also noted that the backwater from the Yangtze River to the Poyang Lake usually lasts for a short time and therefore has minimal effects on the morphology of the lake mouth.

By comparing the bed elevation between the high (Figure 3c) and the low flow conditions (Figure 3d), it is seen that the erosion during the low flow conditions was larger and the thalweg of the post confluence tended to deviate to the right. The mid-stream scour hole near CYP5 of the CHZ (Figures 3c and 3d) displayed typical post-confluence bed morphology. Strong erosion occurred during the low flow conditions, shaped the scour hole into a deep channel on the right side, and was accompanied by large deposition that occurred on the left side. This morphology is similar to that of river bends due to a single helical motion of the flow. At the outflow channel of Poyang Lake, bed elevation decreased from August to December, 2018, probably due to the larger momentum flux of the flow. The bed elevations of the left and right branches of the Yangtze River near the Guan Island had a difference of about 5 m, thereby, this confluence of two branches has a bed discordance. Discordant river confluences are common in braided rivers with mid-channel bars and islands (Szupiany et al., 2009). Bed discordance can enhance the exchange of momentum between two flows (Ramos et al., 2019) and may play a role in the mixing of the left and right branch flows of the Yangtze River. As the maximum water depths of the Yangtze River and the Poyang Lake were similar, this confluence is almost concordant with a negligible effect of bed discordance on the momentum exchange.

Water discharge, sediment load and bed morphology were largely modified by the operation of the Three Gorges Dam. As presented by Qiao et al. (2014) and Guo et al. (2012),

discharge and sediment load during the flood seasons, i.e. from July to September, after the operation of the Three Gorges Dam decreased by 11% to 18% and by 56% to 71%, respectively. Hence, the river impact on the lake weakened in terms of backwater effect and backflow of sediment into the lake. This led to a larger lake inflow into the river decreasing water storage in the lake. Similar results can be discerned in Figure 4, where change in the sediment concentration at Jiujiang and Hukou stations before and after the operation of Three Gorges Dam are shown. Sediment entrapped in the reservoir of Three Gorges Dam decreased TSS concentration downstream of the Dam during the high flow conditions, resulting in erosion of the downstream reach of Yangtze River (Figure 3e-f). The sediment load of the Poyang Lake did not undergo any noticeable change, except for the apparent increases of sediment concentration at Hukou, due to the Yangtze River backwater, which occurred three times in 2000. However, such backwater was not observed in 2015 and 2018 due to the weak forcing effects of the river on the lake.

3.2 Hydraulic conditions during two surveys and depth-averaged flow field

Table 1 lists the main geometric and hydraulic characteristics of the confluence during each of the two surveys. In August Yangtze River discharge was more than twice that in December, with an average water depth 1.42 m larger. Poyang Lake discharge was similar in the two surveys, but the average water depth in August was 0.81 m larger than that in December. This could be attributed to larger backwater effects by the Yangtze River in August. Due to the backwater, the flow in the lake spilled on to the floodplain, widening the width at the water surface and largely decreasing flow velocity in Poyang Lake. The Poyang Lake flow aspect ratio changed from 183 in August to 86 in December. The confluence discharge ratio and flow momentum flux ratio (calculated by the ratio of values of the Poyang Lake to those of the

Yangtze River) both increased from the August high flow condition to the December low flow condition.

Figure 5 shows the depth-averaged velocity data (magnitude and direction) collected at each transect in Survey 1 (Figure 5a) and Survey 2 (Figure 5b). Figure 6 presents the difference in velocity magnitude and flow direction between Yangtze River and Poyang Lake for the two surveys. During Survey 1, flow in the Yangtze River was bifurcated into branches by the Guan Island and then converged downstream. The two branches differed in velocity magnitude, and the difference subsequently deceased as they merged. Conversely in the Poyang Lake, the depth-averaged flow velocity was relatively uniform over the channel width, with a median value of 0.2 m/s. The floodplains on the right side of the Yangtze River and on the left side of the Poyang Lake were submerged in the high flow condition. As the Yangtze River and Poyang Lake entered the confluence, the channel width was almost 3 km, with the two waters merging about a strong and easily visible mixing interface (Figure 7). Through the central confluence region, the waters of the Yangtze River and Poyang Lake merged and realigned with the downstream channel of the Yangtze River flow. Complete alignment of the Poyang Lake flow with the Yangtze River channel occurred at about the CYP7, which was located 3 km downstream of the junction apex (Figure 6). The momentum flux of the Yangtze River was large, its flow moved fast and seemed to rush to the right bank and then near CYP6 abruptly changed its direction to the left bank. The flow vectors from CYP4 to CYP6 swerved rapidly in the anti-clockwise direction by nearly 34 degrees. This abrupt swerve may affect the helical motion over the cross section, as will be discussed below.

During Survey 2, the difference in velocity magnitude between two branches of the Yangtze River was relatively small. Complete alignment of the Poyang Lake flow with the

Yangtze River channel and the largely reduced difference in depth-averaged velocity between the two flows occurred at about CYP6, which was located about 2.4 km downstream of the junction apex (Figure 6). A stagnation zone appeared just downstream of the Meijia Island having a length of about 300 m and a transverse width of about 130 m at CYP1. The confluent flows swerved from CYP4 to CYP6 with an anti-clockwise angle of nearly 25.5 degrees, which was much smaller than during the Survey 1 high flow conditions. This contrast on the flow deflection between the two surveys can be related to the difference in the momentum flux ratios. The flow originating from the Poyang Lake could smoothly change the direction of the flow in Yangtze River to become a part of the core and flow downstream together. The core velocity had gradually increased with the addition of Poyang Lake flow and reached the maximum near CYP8. The flow near CYP9 was affected by the inflow from the left branch at the Zhangjia Island.

3.3 Three-dimensional flow field

Figure 8 shows the vectors of the secondary current velocity superimposed on the contours of the primary flow velocity using the Rozovskii definition for the Survey 1. Figures 9 and 10 compare raw data and those from Rozovski frame for some cross sections. The main stream was flowing along the left branch of the Yangtze River near the Guan Island, and merged with the flow of the right branch at Y1. The flow velocity decreased due to the widening cross section. The flow velocity was distributed almost uniformly over the cross section within the left part of CYP0. The flow fed by the Poyang Lake was much smaller, especially on the floodplain.

The two flows originating from the Yangtze River and the Poyang Lake started to merge at CYP0. Affected by squeezing of the Poyang Lake flow and narrowness of the cross section, the Yangtze River flowincreased its velocity at CYP1. One discernible anti-clockwise cell

emerged on the right side of CYP1 and subsequently two reversed helical cells on either side of the mixing interface developed from CYP2 to CYP4. The incomplete cell or one half of a helix (Lane et al., 2008) in CYP2 might be an artefact due to the nonorthogonality between the transect and the flow direction. The left helical cell with a secondary flow velocity of about 1/10 of the primary velocity at the Yangtze side was related to the curvature of the Yangtze flows (Figure 9), and its relative strengths (e.g., its circulation and the streamwise distance over which it maintained its coherence) depended mainly on the flow curvature and on the momentum flux ratio between the two tributaries (Constantinescu et al., 2011). A large-size helical cell was observed on the right side in CYP1 to CYP3. Such cell should not be attributed to the curvature of the Poyang Lake flow, which was characterized by small flow momentum, but to the penetration of the near-bed Yangtze flow into the Poyang flow (Figure 10). This helical cell lost its size by the time it reached CYP5. An anti-clockwise cell emerged near the right side of CYP6 and continued to move downstream. As mentioned before, we infer that the flow with a large velocity near the surface rushed to the right bank and abruptly changed its direction to the left (Figure 5a), creating such anti-clockwise cell. The topographic steering near the bed, e.g., the swell in the middle of CYP6, may also play a role in generating this cell (Lyubimova et al., 2020). At CYP4 and CYP5 a deep scour hole, 6 m deeper than that at CYP3 and 3 m deeper than that at CYP6, was observed. The hole appeared near CYP3 and increased in size at CYP4, where the core of the maximum velocity was well towards the left side. Its location was not corresponding to the maximum velocity, but it was near the middle of twin helical cells, where the downwelling flow occurred. Downwelling and upwelling flows related to the helical motions can cause pressure difference at the bed, in excess and defect to the hydrostatic pressure

respectively, in rivers, and might be related to the mid-stream scour hole (Rhoads, 1996; Rhoads et al., 2009; Yuan et al., 2018).

Figure 11 shows the vectors of the secondary velocity superimposed on the contours of the primary velocities during Survey 2. Upstream of the confluence, smaller velocities in the Yangtze River were noted as the discharge was much smaller in Survey 2 than in Survey 1. Nonetheless, the velocity in the Poyang Lake outflow channel was much larger during the low flow conditions, when the flow was not submerging the flood plain. A stagnation zone was generated between the two flows at CYP1 and CYP2.

Twin helical cells at two sides of the stagnation zone at CYP1 were small but still discernible. They evolved rapidly into a single, channel-scale circulation, akin to the results of a small confluence of Kaskaskia River and Copper Slough (Bradbrook et al., 2000; Rhoads and Kenworthy, 1995, 1998), despite the different order of magnitude. As in Survey 2 the velocity ratio was about 1 (Table 1), the two tributaries rapidly attained similar flow momentum flux and the velocity got distributed almost uniformly in CYP4. Comparatively, flow velocity homogenization was more rapid in Survey 2 than in Survey (Figure 6). Subsequently, the two flows merged into a single stream and moved along the channel bend as in the classical river bend flow. A single, channel-wide, clockwise secondary circulation occurred. It developed from CYP3 to CYP9 and reached its maximum size at CYP5 and CYP6, where the bend curvature was the largest. Additionally, smaller aspect ratios also helped in mixing, since low water level constrained the flow to take place in a deep channel. The locations of the scour hole at CYP3 and CYP4 were close to the helical cell and the shear layer, and far away from the local maximum velocity. This location is also probably related to various turbulence structures within the shear layer (Best 1987; Sukhodolov and Rhoads, 2001; Rhoads 1996; Rhoads et al., 2009; Yuan et al.,

2018). As the core of maximum velocity was contained in a deep channel, both large flow velocity and secondary cells could generate a deep channel near the right bank, extending from CYP5 towards the downstream, as in bend flows.

3.4 Suspended sediment transport

Figure 1(c-d) shows the depth-averaged suspended sediment concentration during Survey 1 (17 locations) and Survey 2 (20 locations). In Survey 1, both discharge and sediment load were larger in the Yangtze River than in the Poyang Lake outflow. The mixing interface was apparent (Figure 7) and it had a suspended sediment concentration of about 40 mg/L. It appears that the sediment carried by these two streams did not mix well even while reaching CYP6. This is reflected by the low sediment concentration (15 mg/L) observed on the right side of the channel at CYP6, a concentration similar to that of the inflow from Poyang Lake.

In Survey 2, the main branch of the Yangtze River did not convey as much sediment as in the high flow conditions and it had a concentration of only about 30 mg/L. However, the flow in the right branch had large velocity due to lowering of water level and it sustained a larger TSS concentration than was observed during Survey 1 in the high flow conditions. The confluent flows from the two branches increased the velocity in the narrowed cross-section and conveyed a much larger sediment load, probably related to bed sediment resuspension (e.g., 147 mg/L at CYP4). As for the Poyang Lake, the concentration of suspended load was more than 90 mg/L, which was much higher than in Survey 1. In the mixing interface TSS concentration was about 80 mg/L. The sediments in these flows got mixed at CYP6 and the concentration dropped to 50 mg/L, much lower than the incoming concentration from Poyang Lake. Some locations were also selected to measure the grain size of the suspended load and bed material in Survey 2 (Figure 12). Yangtze River and Poyang Lake had similar median grain sizes of the suspended load.

Poyang Lake was likely transporting only silt (with 83% of the particles less than 0.05 mm) and clay (with 12% of particles less than 0.002 mm) in suspension during Survey 2. However, Yangtze River was transporting some fine sand (with 18% of particles larger than 0.05 mm) as well as silt (silt comprising 82% and without clay) (Figure 12). The grain size of bed material differed markedly between each channel. Poyang Lake had much finer bed material than that of the Yangtze River, and its median grain size was only 50 μm. Therefore, the Poyang Lake channel carried more suspended load and was subjected to severe erosion during the high-velocity periods of Survey 2 (Figure 3d).

Figure 13 shows the spatial variation of TSS concentration (represented by values of *RB*) for Survey 1. The two branches of the Yangtze River merged and mixed their masses, including the suspended load. The two branches of the Yangtze River joined together and came to the almost uniform axial velocity in the left part of CYP0 (Figure 8). The mixing of suspended sediment was not quite complete further downstream at CYP1. The mixing of Yangtze and Poyang Lake sediment was also impeded, with little mixing before CYP5 and full mixing not apparent until CYP9 section, downstream of the CHZ. Apparently it was difficult for Yangtze River sediment to move laterally across the downwelling flow of the shear layer. Suspended sediment transport was likely affected by the helical motion and moved along the flank of the scour hole. A deep scour hole, having very little sediment concentration in it, was well maintained. The highest concentration of sediment was transported along the flanks of the scour hole; as a consequence, the scour hole was not filled up. Similar observations were made on movement of bed load in the laboratory by Mosley (1976) and Best (1988), as well as in a small river confluence by Boyer et al. (2006). Suspended load in a large braid-bar confluence (Szupiany et al., 2009) also exhibited similar features. The clockwise secondary cell on the left

side restricted the movement of the suspended sediment, until an anti-clockwise secondary cell appeared at CYP6 and nullified this constraint and the core of sediment was pushed to the right side. As a result, it was not possible to maintain the scour hole observed at CYP4 and CYP5 any further. Besides the effects of the helical motions, the shear-driven turbulence within the mixing interface may also affect the mixing of suspended sediment between two flows (Lane et al., 2008). The frequency of these KH vortices within the shear layer was about 20 s (Figure 7), and their sizes were about 20 m by drone observations. Compared with the river width, the scale of shear-driven turbulence might not have a significant effect on the mixing. Lane et al. (2008) also presented the similar conclusion that mixing driven by turbulent shear associated with a near-vertical shear layer was restricted close to the junction.

Figure 14 shows the spatial distribution of TSS concentration (represented by values of *RB*) in Survey 2. The left branch of the Yangtze River, with a low sediment concentration, merged with the right branch and the sediment was well mixed at CYP0. As for mixing of the Yangtze and Poyang Lake flows, just as in Survey 1, the channel-size secondary cell prevented the highest sediment concentration to move across the flow. Thus, transport of sediment to the right side was impeded. Without this effect from the downwelling flow, the sediment could have moved over the deepest part of the channel preventing the development of the scour hole. Because of downwelling flow, even at CYP8, the sediment could not be distributed uniformly across the section. In this case, a local scour hole was not formed as the channel-size secondary cell emerged, leading instead to the formation of a deep bent channel.

3.5 Depth-averaged flow velocity and suspended load

Figure 15 shows the spatial distribution of depth-averaged TSS concentration (represented by *RB*) and depth-averaged flow velocity at the confluence for two surveys. These

distributions were not always each other consistent. The depth-averaged momentum flux represents the ability of the primary flow to carry sediment. Sediment concentration was also largely determined by secondary currents, and turbulent diffusion, as well as by entrainment from the bed. The mismatch between the velocity and the sediment concentration reflects some fundamental differences between the transport mechanisms of momentum and sediment. It could be due to the presence of the secondary currents and to a lesser degree other types of large-scale coherent structures (e.g., the shear-driven KH instabilities at the mixing interface).

From the two surveys, it can be seen that the distributions of flow velocity and sediment concentration are more consistent in Survey 1. Inconsistency emerged mainly at CYP5 and CYP6, where the velocity was uniform, whereas the highest TSS concentration was confined to the left side, apparently by the presence of the clockwise helical cell, looking downstream. After CYP6, the sediment moved laterally to the right side and was gradually mixed, likely because of the anti-clockwise cell. In contrast, in Survey 2, they were less related over the stretch extending up to CYP8 because of the channel-size secondary cell.

3.6 Discussion

So far, the bed morphology, flow dynamics and suspended sediment transport at the large channel confluence of the Yangtze River and the Poyang Lake outflow were presented separately. In this Section, they are comparatively discussed with those observed in previous studies (e.g., Best, 1987, 1988; Boyer et al., 2006; Parsons et al., 2007; Parsons et al., 2008; Lane et al, 2008; Szupiany et al., 2009; Constantinescu et al., 2011).

A conceptual model for flow dynamics at channel confluences was proposed by Best (1987), which consisted of six distinct regions: flow stagnation, flow deflection, flow separation, maximum velocity, gradual flow recovery and the shear layer. In this study, most of these flow

features were found, barring the zone of flow separation. In a flume confluence with a sharp angle (e.g., Yuan et al., 2018), it was easy to find a separation zone as a tributary enters the main channel. However, in a natural river confluence flow usually cannot separate from the relatively streamlined bank (Constantinescu et al., 2011). Though the flow does not separate from the bank, the strong bank curvature may induce the formation of a thin shear layer of high vorticity, separating the core of high streamwise velocity from the region of low streamwise velocity near the bank (Constantinescu et al., 2011). That there was a wide region of low streamwise velocity between the left bank and the core of high streamwise velocity (from location CYP1 to CYP5) confirms the occurrence of such a phenomenon in Yangtze River. A stagnation zone was discernible at CYP0 in Survey 1 and also over a large area of CYP0 and CYP1 in Survey 2. In Survey 2, both flows, having similar momentum flux, are able to separate from the inside banks to form a large stagnation zone when the confluence angle is large. Downstream of the stagnation zone, eddies from each flow were alternately shed into the mixing interface and develop into quasi-2D vortices (Figure 7). This process is similar to the vortex shedding responsible for the development of vortex pairing (Kirkil and Constantinescu, 2009).

It was commonly accepted that the secondary flows were weak and spatially constrained in large rivers due to large width-to-depth ratios. The occurrence of dual, counterrotating helical cells was documented in field studies of small river confluences (Rhoads, 1996; Rhoads and Kenworthy, 1998; Rhoads and Sukhodolov, 2001; Constantinescu et al., 2011). Very weak helical cells were also observed in a large braided-bar confluence (Szupiany et al., 2009). Twin surface-convergent helical cells on either side of a mixing interface in the vertical plane were observed, and were attributed to the curvature of the two combining flows (Bradbrook et al., 2000; Rhoads & Kenworthy, 1995, 1998; Sukhodolov and Sukhodolova, 2019). It was important

to note that streamwise-oriented vortical cells, induced by the presence of a large junction angle, were not related to the secondary instability that developed along the core of the KH rollers within the mixing interface (Constantinescu et al., 2011). Their development was largely affected by the planform of the downstream channel. The post confluence flows contained a single channel-size circulation because of the curvature of the river planform. The curvature of the downstream river planform and the momentum flux of the confluent flows mainly determined the strength of this channel-size circulation and the streamwise distance over which it maintains coherence. In the present study, having large ratios of width to depth, this kind of channel-size circulation was also observed in Survey 2. This study captured the evolution process of dual helical cells when two flows had a large difference in flow momentum flux. One helical cell was caused by the curvature of the Yangtze River with a large flow momentum; while the other helical cell was generated by the penetration of its flows into the Poyang Lake flows. The momentum flux of the Poyang Lake flow by itself was too small to cause such a large helical cell. Furthermore, this helical cell mostly decayed as the lateral uniform velocity occurred near CYP5, while the helical cell caused by the curvature of the Yangtze River got stronger because of the larger curvature there. Another interesting observation is that a large anti-clockwise helical cell occurred near CYP6 which was likely related to the substantial deflection of the flow or topographic steering near the bed because of river planform. In due course of time it grew into a channel-size circulation.

In summary, in spite of the ratio of width to depth being large, large-size secondary circulations were observed in this study. They were mainly attributed to the curvature of the Yangtze River at the confluence and the penetration of its flow into the Poyang Lake flow. The secondary circulations caused by the flow penetration are much larger than previously observed

in Rio Paraná confluences, where the small curvature of the main stream restricted the secondary motions observed by Szupiany et al. (2009), and the dune roughness (approaching 2.2 m) scaling with the flow depth (~7 m), the small curvature of the main stream, and the pronounced bed discordance (the tributary being up to 6 meters shallower than the main stream) could all have affected the occurrence of the secondary circulations observed by Parsons et al. (2007).

Previous studies in large river confluences have found the influence of the helical motions on the sediment transport and bed morphology to be small. They correlated the sediment transport process with the turbulence level of flow. Based on laboratory studies it has been reported, qualitatively (Mosley, 1976) as well as quantitatively (Best, 1988), that the largest bed load transport pathway occurred essentially around the periphery of the scour hole. This in turn helps to maintain the scour hole. For a small river confluence, high transport rate of bed load occurred at the edges of the shear layer region where horizontal□vertical cross stresses were high (Boyer et al., 2006). It was also observed that erosion occurs along the shear layer, which matched with changes noticed in the bed morphology. Highest concentrations of suspended sediment in large river confluence were found along the flank of the scour hole lying within the two enjoining flows (Szupiany et al., 2009). They suggested that the phenomenon is related to the high turbulence levels of the shear layer. In larger channel confluences, however, the secondary currents may be too weak and/or spatially restricted to have any significant influence on these cores of high sediment concentration. Nonetheless, Lane et al. (2008) indicated that the large-size secondary circulation was beneficial to the rapid mixing of two large confluent rivers. In the present study, channel size secondary currents appeared to affect suspended sediment transport. The upstream regions of higher velocity of the Yangtze River control the sediment input, which then moves along a distinct corridor on the left of the downstream channel. The

helical motions on the left side restricted the size of the core of high sediment concentration, while the downwelling flows acted as a barrier preventing sediment mixing between the two rivers. Although the reverse helical motion observed at CYP6 during the high flow condition did not impede the sediment mixing, its enhancement of mixing was comparatively small. The secondary flow velocity was one order of magnitude smaller than the primary flow velocity, i.e. the lateral movement of water particles and sediment was much slower compared with the streamwise movement, and thus the complete mixing occurred downstream of the confluence zone, at CYP9. The KH vortices within the shear layer caused by shear driven turbulence are considered as a factor for water mixing between two confluent flows. However, their influence depends on the frequency of shedding and the scale of the vortex. In this study, it is expected that their effect was limited as their sizes were two orders of magnitude smaller than the river width. Furthermore, their strengths largely decayed as the velocity difference between the two streams gradually decreased downstream.

As regards the bed morphology of the river confluence, many field surveys (Biron et al., 1993; Boyer et al., 2006; Rhoads et al., 2009) and laboratory experiments (Best, 1988; Guillén-Ludeña et al., 2015, 2016; Leite Ribeiro et al., 2012) on sediment transport and morphology at river confluences were conducted in the past. Quite a few hypotheses were proposed for the origin of the mid-stream scour hole, such as the large flow velocity, strong turbulence, the effect of the shear layer or the curvature-induced helical circulation (Best, 1988; Guillén-Ludeña et al., 2015, 2016; Leite Ribeiro et al., 2012; Rhoads et al., 2009; Sukhodolov & Rhoads, 2001). Recent work by Yuan et al. (2018) showed that the intense shear towards the bed by downwelling and upwelling flows, resulting from helical motions were responsible for the mid-stream scour hole in a flume confluence. This conclusion also seems to be reasonable to explain the bed

morphology observed herein. The local scour hole might be related to the twin helical motions with the downwelling flows in the middle, as they could allow the movement of sediment to take place along the flanks of the hole, thereby helping to maintain the hole. A long-surviving helical cell, just like the one induced by the bend planform in Survey 2, could lengthen the hole into a deep channel. The hole disappeared downstream when the helical motions weakened, or when a reverse helical cell occurred, in Survey 1.

4 Conclusions

Two field surveys were conducted to investigate hydrodynamics, suspended sediment transport and morphological features of a large river confluence between the Yangtze River (the largest river in China) and the outflow channel of Poyang Lake (the largest freshwater lake in China). The main important conclusions drawn from this study are:

(1) The operation of the Three Gorges Dam is responsible for the erosion of the Yangtze River channel near the confluence apex. It did not affect the bed elevation of the Poyang Lake outflow channel.

(2) The confluence of the Yangtze River and the Poyang Lake outlet is almost concordant. Mixing of flow momentum and suspended sediment were relatively slow, especially during high flow conditions.

(3) Channel-size secondary flows, like the dual counter-rotating cells in high flow conditions and a single secondary cell during low flow conditions, were observed near the confluence. This contrasts the common belief that the scale of the helical cells should get

constrained because of an increase in the form roughness associated with large width-to-depth ratio of the channel.

(4) Occurrence of these helical cells was mainly attributed to the curvature of the main stream and the penetration of the main flow into the flow from the tributary. The helical cells caused by the latter are much stronger than those related to the former.

(5) The helical motions restrained the core size of high sediment concentration, while the downwelling flows acted as a partition that prevented the mixing of sediment carried by the two rivers. Depending on the frequency of shedding and the scale of the vortex, the effects of the shear-driven turbulence within the mixing interface appeared limited, although turbulence data would be needed to confirm this.

(6) The local scour hole was likely related to the twin helical motions with the downwelling flows in the middle, as they could restrict the movement of sediment to take place along the flanks of the hole, thereby helping to maintain the hole. A long-surviving helical cell was likely beneficial to stretch the hole to form a deep channel.

(7) During the low flow conditions, the scour hole disappeared downstream as the helical motion became weaker. In high flow conditions, a reverse helical cell enhancing sediment mixing and affecting the development of the scour hole was observed.

(8) This large river confluence exhibited a strong interaction among the different hydro-morpho-sedimentary processes. Channel planform and the discharge ratio affected the flow dynamics, especially the helical motion. The helical motion near the CHZ impacted sediment transport and, thus, local bed morphology.

Acknowledgments

This research was funded by the National Natural Science Foundation of China (52079044; 51779080), the Fundamental Research Funds for the Central Universities (B200202237), the 111 Project (B17015), and the Fok Ying Tung Education Foundation (520013312). The authors would like to thank Professor Bidya Sagar Pani of the Indian Institute of Technology-Bombay and Professor Zhaoyin Wang of Tsinghua University for help in revising this work. Thanks are also extended to the Hydrology and Water Resources Survey Bureau of the Lower Reaches of the Yangtze River for data support, and Shujun Huang, Ming Gao, Kun Zhang, Qingwei Lin, Guolong Zhao, and Hao Wang of Hohai University for their support during the field surveys. The authors would like to thank three anonumous reviewers, and editors for their valuable comments and suggestions.

Data availability statement

The data are available for download at Researchgate (http://doi.org/10.13140/RG.2.2.12785.10084; http://doi.org/10.13140/RG.2.2.29562.31684; http://doi.org/10.13140/RG.2.2.31240.03841; http://doi.org/10.13140/RG.2.2.27884.59526; http://doi.org/10.13140/RG.2.2.15301.68327).

References

Baranya, S., Olsen, & N. R. B., Józsa, J. (2015). Flow analysis of a river confluence with field measurements and RANS model with nested grid approach. *River Research and Applications*, 31(1): 28–41. doi: 10.1002/rra.2718.

Baranya, S., & Józsa, J. (2013). Estimation of suspended sediment concentrations with ADCP in Danube River. *Journal of Hydrology and Hydromechanics*, 61(3), 232–240. doi: 10.2478/johh-2013-0030.

Best, J. L. (1987). Flow dynamics at river channel confluences: Implications for sediment transport and bed morphology, in Recent Developments in Fluvial Sedimentology, edited by F. G. Ethridge et al. The Society of Economic Paleontologists and Mineralogists, 39, 27–35. doi:10.2110/pec.87.39.0027.

Best, J. L. (1988). Sediment transport and bed morphology at river channel confluences. *Sedimentology*, 35, 481–498. doi:10.1111/j.1365-3091.1988.tb00999.x.

Best, J. L., & Ashworth, P. J. (1997). Scour in large braided rivers and the recognition of sequence stratigraphic boundaries. *Nature*, 387, 275–277. doi: 10.1038/387275a0.

Biron, P. M., Buffin-Bélanger, T., & Martel, N. (2019). Three-dimensional turbulent structures at a medium-sized confluence with and without an ice cover. *Earth Surface Processes and Landforms*, 44(15), 3042–3056. doi:10.1002/esp.4718.

Biron, P., Roy, A. G., Best, J. L., & Boyer C. J. (1993). Bed morphology and sedimentology at the confluence of unequal depth channels. *Geomorphology*, 8, 115–129. doi:10.1016/0169-555X (93)90032-W.

Biron, P., & Lane, S. (2008). Modelling hydraulics and sediment transport at river confluences, in River Confluences. Tributaries and the Fluvial Network, edited by S. P. Rice, A. G. Roy, and B. L. Rhoads, J. Wiley &Sons, Ltd. ISBN: 978-0-470-02672-4, 17–43.

Biron, P., Roy, A. G., & Best, J. L. (1996a). Effects of bed discordance on flow dynamics at open channel confluences. *Journal of Hydraulic Engineering*, 122, 676–682. doi:10.1061/(ASCE)0733-9429(1996)122:12(676)

Biron, P., Roy, A. G., & Best, J. L. (1996b). Turbulent flow structure at concordant and discordant openchannel confluences. *Experiments in Fluids*, 21, 437–446. doi:10.1007/BF00189046

Boyer, C., Roy, A. G., & Best, J. L. (2006). Dynamics of a river channel confluence with discordant beds: Flow turbulence, bed load sediment transport, and bed morphology. *Journal of Geophysical Research*, 111, F04007. doi:10.1029/2005JF000458.

Bradbrook, K. F., Biron, P. M., Lane, S. N., Richards, K. S., & A. G. Roy (1998). Investigation of controls on secondary circulation in a simple confluence geometry using a three-dimensional numerical model. *Hydrological Processes*, 12: 1371–1396. doi:10.1002/(SICI)1099-1085(19980630)12:8<1371::AID-HYP620>3.0.CO;2-C.

Bradbrook, K. F., Lane, S. N., & Richards, K. S. (2000). Numerical simulation of three□dimensional time□averaged flow at river channel confluences. *Water Resources Research*, 36(9), 2731–2746. doi:10.1029/2000WR900011.

Bradbrook, K.F., Lane, S. N., Richards, K. S., Biron, P., & Roy, A. G. (2001). Role of bed discordance at asymmetrical open-channel confluences. *Journal of Hydraulic Engineering*, 127(5), 351–368. doi: 10.1061/(ASCE)0733-9429(2001)127:5(351).

Cheng Z., & Constantinescu, G. (2018). Stratification effects on flow hydrodynamics and mixing at a confluence with a highly discordant bed and a relatively low velocity ratio. *Water Resources Research*, 54(7), 4537–4562. doi:10.1029/2017WR022292.

Constantinescu, G., Miyawaki, S., Rhoads, B., & Sukhodolov A. (2012). Numerical analysis of the effect of momentum ratio on the dynamics and sediment entrainment capacity of coherent flow structures at a stream confluence. *Journal of Geophysical Research: Earth Surface*, F4, F04028. doi:10.1029/2012JF002452.

Constantinescu, G., Miyawaki, S., Rhoads, B., Sukhodolov A., & Kirkil, G. (2011). Structure of turbulent flow at a river confluence with momentum and velocity ratios close to 1: Insight provided by an eddy resolving numerical simulation. *Water Resources Research*, 5, W05507. doi:10.1029/2010WR010018.

Creed, E. L., Pence, A. M., & Rankin, K. L. (2001). Inter-comparison of turbidity and sediment concentration measurement from an ADP, an ABS-3, and a LISST, in Oceans 2001 MTS/IEEE Conference Proceedings, vol. 3, pp. 1750–1754, Honolulu, Hawaii. DRL Software Ltd (2003), DRL-Sediview software user manual V3, DRL Software Ltd.

De Serres, B., Roy, A. G., Biron, P., & Best, J. L. (1999). Three-dimensional structure of flow at a confluence of river channels with discordant beds. *Geomorphology*, 26(4), 313–335. doi: 10.1016/S0169-555X(98)00064-6.

Filizola, N., & Guyot, J. L. (2004). The use of Doppler technology for suspended sediment discharge determination in the River Amazon. *Hydrological Sciences Journal*, 49, 143–153. doi:10.1623/hysj.49.1.143.53990.

Gualtieri C., Ianniruberto, M., & Filizola, N. (2019). On the mixing of rivers with a difference in density: the case of the Negro/Solimões confluence, Brazil. *Journal of Hydrology*, 578(11), 124029. doi:10.1016/j.jhydrol.2019.124029

Gualtieri, C., Filizola, N., de Oliveira, M., Santos, A. M., & Ianniruberto, M. (2018). A field study of the confluence between Negro and Solimões Rivers. Part 1: Hydrodynamics and sediment transport. *Comptes Rendus Geoscience*, 350(1–2), 31–42. doi:10.1016/j.crte.2017.09.015.

Guillén-Ludeña, S., Franca, M. J., Cardoso, A. H., & Schleiss, A. J. (2015). Hydro□ morphodynamic evolution in a 90°movable bed discordant confluence with low discharge ratio. *Earth Surface Processes and Landforms*, 40(14), 1927–1938. doi:10.1002/esp.3770.

Guillén-Ludeña, S., Franca, M. J., Cardoso, A. H., & Schleiss, A. J. (2016). Evolution of the hydromorphodynamics of mountain river confluences for varying discharge ratios and junction angles. *Geomorphology*, 255, 1–15. doi:10.1016/j.geomorph.2015.12.006.

Guillén Ludeña, S., Cheng, Z., Constantinescu, G., & Franca, M. J. (2017). Hydrodynamics of mountain□river confluences and its relationship to sediment transport. *Journal of Geophysical Research: Earth Surface*, 122(4), 901–924. doi:10.1002/2016JF004122.

Guo, H., Hu, Q., Zhang, Q., & Feng, S. (2012). Effects of the three gorges dam on Yangtze river flow and river interaction with Poyang Lake, China: 2003–2008. *Journal of Hydrology*, 416, 19–27. doi:10.1016/j.jhydrol.2011.11.027.

Ianniruberto, M., Trevethan, M., Pinheiro, A., Andrade, J. F., Dantas, E., Filizola, N., Santos, A., & Gualtieri, C. (2018). A field study of the confluence between Negro and Solimões Rivers. Part 2: Bed morphology and stratigraphy. *Comptes Rendus Geoscience*, 350(1–2), 43–54. doi:10.1016/j.crte.2017.10.005.

Kirkil, G., & Constantinescu, G. (2009). Nature of flow and turbulence structure around an in stream vertical plate in a shallow channel and the implications for sediment erosion, *Water Resources Research*, 45, W06412. doi:10.1029/2008WR007363.

Konsoer, K. M., & Rhoads, B. L. (2014). Spatial–temporal structure of mixing interface turbulence at two large river confluences. *Environmental Fluid Mechanics*, 14(5), 1043–1070. doi:10.1007/s10652-013-9304-5.

Kostaschuk, R., Best, J., Villard, P., Peakall, J., & Franklin, M. (2005). Measuring flow velocity and sediment transport with an acoustic Doppler current profiler. *Geomorphology*, 68(1–2), 25–37. doi:10.1016/j.geomorph.2004.07.012.

Lane, S. N., Bradbrook, K. F., Richards, K. F., Biron, P. M., & Roy, A. G. (1999). Time-averaged flow structure in the central region of a stream confluence: a discussion. *Earth Surface Processes and Landforms*, 24(4), 361–367. doi: 10.1002/(SICI)1096-9837(199904)24:4<361::AID-ESP982>3.0.CO;2-5.

Lane, S. N., Bradbrook, K. F., Richards, K. F., Biron, P. M., & Roy, A. G. (2000). Secondary circulation cells in river channel confluence: measurement artefacts or coherent flow structures? *Hydrological Processes*, 14(11–12), 2047–2071. doi: 10.1002/1099-1085(20000815/30)14:11/12<2047::AID-HYP54>3.0.CO;2-4.

Lane, S.N., Parsons, D. R., Best, J. L., Orfeo, O., Kostachuk, R., & Hardy, R. J. (2008). Causes of rapid mixing at a junction of two large rivers: Rio Paraná and Rio Paraguay, Argentina. *Journal of Geophysical Research*,113(F2), F02024. doi:10.1029/2006JF000745.

Leite Ribeiro, M., Pfister, M., Schleiss, A. J., & Boillat, J. L. (2012). Hydraulic design of A-type Piano Key Weirs. *Journal of Hydraulic Research,* 50(4): 400–408. doi: 10.1080/00221686.2012.695041.

Luz, L. D., Szupiany, R. N., Parolin, M., Silva, A., & Stevaux, J. C. (2020). Obtuse-angle vs. confluent sharp meander bends: insights from the Paraguay-Cuiabá confluence in the tropical Pantanal wetlands, Brazil. *Geomorphology*, 348, 106907. doi:10.1016/j.geomorph.2019.106907.

Lehner, B., Liermann, C. R., Revenga, C., Vörösmarty, C., Fekete, B., Crouzet, P., Döll, P., Endejan, M., Frenken, K., Magome, J., Nilsson, C., Robertson, J. C., Rödel, R., Sindorf, N., & Wisser, D. (2011). Global Reservoir and Dam Database, Version 1.1 (GRanDv1): Reservoirs, Revision 01, NASA Socioecon. Data and Appl. Cent., Palisades, N. Y., doi:10.7927/H4HH6H08.

Lyubimova, T., Lepikhin A., Konovalov, V., Parshakova, Ya., & Tiunov A. (2014). Formation of the density currents in the zone of confluence of two rivers. *Journal of Hydrology*, 508, 328–342. doi: 10.1016/j.jhydrol.2013.10.041

Lyubimova, T. P., Lepikhin, A. P., Parshakova, Y. N., Kolchanov, V. Y., Gualtieri, C., Roux, B., & Lane, S. N. (2020) A numerical study of the influence of channel-scale secondary circulation on mixing processes downstream of river junctions. *Water*, 12, 2969; doi:10.3390/w12112969

Martín-Vide, J. P., Plana-Casado, A., Sambola, A., & Capapé, S. (2015). Bed load transport in a river confluence. *Geomorphology*, 250, 15–28. doi: 10.1016/j.geomorph.2015.07.050

Moradi, G., Vermeulen, B., Rennie, C. D., Cardot, R., & Lane, S. N. (2019). Evaluation of aDcp processing options for secondary flow identification at river junctions. *Earth Surface Processes and Landforms*, 44(14), 2903–2921. doi:10.1002/esp.4719.

Mosley, M. P. (1976). An experimental study of channel confluences. *The Journal of Geology*, 84(5), 535–562. Retrieved from http://www.jstor.org/stable/30066212.

Parsons, D. R., Best, J. L., Lane, S. N., Orfeo, O., Hardy, R. J., & Kostaschuk, R. (2007). Form roughness and the absence of secondary flow in a large confluence–diffluence, Rio Paraná, Argentina. *Earth Surface Processes and Landforms*, 32(1), 155–162. doi:10.1002/esp.1457.

Parsons, D. R., Best, J. L., Lane, S. N., Kostachuk R. A., Hardy, R. J., Orfeo, O., Amsler M. L., & Szupiany, R. N. (2008), Large river channel confluences, In River Confluences, Tributaries and the Fluvial Network, edited by S. P. Rice, A. G. Roy, and B. L. Rhoads, J. Wiley &Sons, Ltd. ISBN: 978-0-470-02672-4, 73–91.

Parsons, D. R., Jackson, P. R., Czuba, J. A., Engel, F. L., Rhoads, B. L., Oberg, K. A., Best, J. L., Mueller, D. S., Johnson, K. K., & Riley, J. D. (2013). Velocity Mapping Toolbox (VMT): a processing and visualization suite for moving□vessel ADCP measurements. *Earth Surface Processes and Landforms*, 38(11), 1244-1260. doi:10.1002/esp.3367

Qiao, H., Zhang, Z., Zhu, Q., & Bu, D. (2014). Variation on characteristics of runoff and sediment discharge of Datong Hydrological Station before and after impoundment of Three Gorges Reservoir. *Water Resource Power*, 2014, 32(9), 24–27. (In Chinese)

Ramón, C., Hoyer, A. B., Armengol, J., & Dolz, J. (2013). Mixing and circulation at the confluence of two rivers entering a meandering reservoir. *Water Resources Research*, 49(3): 1429–1445. doi: 10.1002/wrcr.20131.

Ramos, P. X., Schindfessel, L., Pego, J. P., & Mulder, T. D. (2019). Influence of bed elevation discordance on flow patterns and head losses in an open-channel confluence. *Water Science and Engineering*, 12(3), 235-243. doi: 10.1016/j.wse.2019.09.005

Rennie, C. D., Millar, R. G., & Church, M. A. (2002). Measurement of bed load velocity using an acoustic Doppler current profiler. *Journal of Hydraulic Engineering*, 128(5), 473-483. doi:10.1061/(ASCE)0733-9429(2002)128:5(473).

Rhoads, B. L. (1996). Mean structure of transport-effective flows at an asymmetrical confluence when the main stream is dominant. In: Ashworth, P.J., Bennett, S.J., Best, J.L., McLelland, S.J. (Eds.), Coherent Flow Structure in Open Channels. John Wiley & Sons Ltd., Chichester, UK, pp. 491–517.

Rhoads, B. L., & Kenworthy, S. T. (1995). Flow structure at an asymmetrical stream confluence. *Geomorphology*, 11(4), 273–293. doi:10.1016/0169-555X(94)00069-4.

Rhoads, B. L., & Kenworthy, S. T. (1998). Time□averaged flow structure in the central region of a stream confluence. *Earth Surface Processes and Landforms*, 23(2), 171–191. doi:10.1002/(SICI)1096-9837(199802)23:2<171::AID-ESP842>3.0.CO;2-T.

Rhoads, B. L., & Kenworthy, S. T. (1999). On secondary circulation, helical motion andRozovskii□based analysis of time□averagedtwo□dimensional velocity fields at confluences. *Earth Surface Processes and Landforms*, 24(4), 369–375. doi:10.1002/(SICI)1096-9837(199904)24:4<369::AID-ESP983>3.0.CO;2-F.

Rhoads, B. L., & Sukhodolov, A. N. (2001). Field investigation of three□dimensional flow structure at stream confluences: 1. Thermal mixing and time□averaged velocities. *Water Resources Research*, 37(9), 2393–2410. doi:10.1029/2001WR000316.

Rhoads, B. L., & Sukhodolov, A. N. (2004). Spatial and temporal structure of shear layer turbulence at a stream confluence. *Water Resources Research*, 40(6), W06304. doi:10.1029/2003WR002811.

Rhoads, B. L., & Sukhodolov, A. N. (2008). Lateral momentum flux and the spatial evolution of flow within a confluence mixing interface. *Water Resources Research*, 44(8), W08440. doi:10.1029/2007WR006634.

Rhoads, B. L., Riley, J. D., & Mayer, D. R. (2009). Response of bed morphology and bed material texture to hydrological conditions at an asymmetrical stream confluence. *Geomorphology*, 109(3-4), 161–173. doi:10.1016/j.geomorph.2009.02.029.

Rhoads, B. L., & Johnson, K. K. (2018). Three-dimensional flow structure, morphodynamics, suspended sediment, and thermal mixing at an asymmetrical river confluence of a straight tributary and curving main channel. *Geomorphology*, 323, 51–69. doi: 10.1016/j.geomorph.2018.09.009.

Riley, D.J. & Rhoads, B.L. (2011). Flow structure and channel morphology at a natural confluent meander bend. *Geomorphology*, 163(SI), 84-98. doi: 10.1016/j.geomorph.2011.06.011.

Riley, J. D., Rhoads, B. L., Parsons, D. R., & Johnson, K. K. (2014). Influence of junction angle on three□dimensional flow structure and bed morphology at confluent meander bends during different hydrological conditions. *Earth Surface Processes and Landforms*, 40(2), 252–271. doi: 10.1002/esp.3624.

Rozovskii, I. L. (1957), Flow of water in bends of open channels, Academy of Sciences of the Ukrainian SSR: Kiev (translated from Russian by the Israel Program for Scientific Translations, Jerusalem,1961).

Sontek (1997), Sontek Doppler Current Meters - Using Signal Strength Data to Monitor Suspended Sediment Concentration, Sontek Application Note, San Diego, Calif.

Stone, R (2008), Three Gorges Dam: into the unknown, *Science*, 321(5889), 628–632, doi:10.1126/science.321.5889.628.

Sukhodolov, A. N., & Sukhodolova, T. A. (2019). Dynamics of Flow at Concordant Gravel Bed River Confluences: Effects of Junction Angle and Momentum Flux Ratio. *Journal of Geophysical Research: Earth Surface*, 124(2), 588-615. doi.org/10.1029/2018JF004648

Sukhodolov, A. N., Krick, J., Sukhodolova, T. A., Cheng, Z., Rhoads, B. L., & Constantinescu, G. S. (2017). Turbulent flow structure at a discordant river confluence: Asymmetric jet dynamics with implications for channel morphology. *Journal of Geophysical Research: Earth Surface*, 122(6), 1278-1293. doi:10.1002/2016JF004126.

Sukhodolov, A. N., & Rhoads, B. L. (2001). Field investigation of three□dimensional flow structure at stream confluences: 2. Turbulence. *Water Resources Research*, 37(9), 2411-2424. doi:10.1029/2001WR000317.

Szupiany, R. N., Amsler, M. L., Parsons, D. R., & Best, J. L. (2009). Morphology, flow structure, and suspended bed sediment transport at two large braid□bar confluences. *Water Resources Research*, 45(5),W05415. doi:10.1029/2008WR007428.

Tang, H., Zhang, H., & Yuan, S. (2018). Hydrodynamics and contaminant transport on a degraded bed at a 90-degree channel confluence. *Environmental Fluid Mechanics*, 18(2), 443-463. doi:10.1007/s10652-018-9612-x.

Winant, C. D., & Browand, F. K. (1974). Vortex pairing: the mechanism of turbulent mixing-layer growth at moderate Reynolds number. *Journal of Fluid Mechanics*, 63(2), 237-255. doi:10.1017/S0022112074001121.

Xu, D., Xiong, M., & Zhang, J. (2001), Analysis on hydrologic characteristics of Poyang Lake. *Yangtze River*, 32(2), 21–27. (in Chinese).

Yu, Q., Yuan, S., & Rennie, C. D. (2020). Experiments on the morphodynamics of open channel confluences: Implications for the accumulation of contaminated sediments. *Journal of Geophysical Research: Earth Surface*, 125(9), e2019JF005438. doi: 10.1029/2019JF005438

Yang, Z. S., Wang, H. J., Saito, Y., Milliman, J. D., Xu, K., Qiao, S., & Shi, G. (2006). Dam impacts on the Changjiang (Yangtze) River sediment discharge to the sea: the past 55 years and after the Three Gorges Dam. *Water Resources Research*, 42(4), W04407. doi: 10.1029/2005WR003970.

Yuan, S., Tang, H., Xiao, Y., Qiu, X., & Xia, Y. (2018). Water flow and sediment transport at open-channel confluences: an experimental study. *Journal of Hydraulic Research*, 56(3), 333-350. doi:10.1080/00221686.2017.1354932.

Yuan, S., Tang, H., Xiao, Y., Xia, Y., Melching, C., & Li, Z. (2019). Phosphorus contamination of the surface sediment at a river confluence. *Journal of Hydrology*, 573, 568–580. doi:10.1016/j.jhydrol.2019.02.036.

Yuan, S., Tang, H., Xiao, Y., Qiu, X., Zhang, H., & Yu, D. (2016). Turbulent flow structure at a 90-degree open channel confluence: Accounting for the distortion of the shear layer. *Journal of Hydro-environment Research*, 12, 130–147. doi:10.1016/j.jher.2016.05.006.

Zheng, S., Xu, Y. J., Cheng, H., Wang, B., Xu, W., & Wu, S. (2018). Riverbed erosion of the final 565 kilometers of the Yangtze River (Changjiang) following construction of the Three Gorges Dam. *Scientific Reports*, 8(1), 1–11. doi: 10.1038/s41598-018-30441-6.

Zhou, Y., Jeppesen, E., Li, J., Zhang, Y., Zhang, X., & Li, X. (2016). Impacts of Three Gorges Reservoir on the sedimentation regimes in the downstream-linked two largest Chinese freshwater lakes. *Scientific Reports*, 6, 35396. doi: 10.1038/srep35396.

Zinger, J. A., Rhoads, B. L., Best, J. L., & Johnson, K. K. (2013). Flow structure and channel morphodynamics of meander bend chute cutoffs: A case study of the Wabash River, USA. *Journal of Geophysical Research: Earth Surface*, 118(4), 2468–2487. doi:10.1002/jgrf.20155.

Figures Caption List

Figure 1. Map of Yangtze River basin indicating the location of the confluence between Yangtze River and the Poyang Lake at the middle and lower reach of the Yangtze River (near 29.75N, 116.22E) (a) and the locations of hydrological stations and islands (b); and measurement setup at the confluence: (c) Survey 1 during the high flow conditions in 10-14 August 2018; (d) Survey 2 during the low flow conditions in 8-12 December 2018. The yellow lines mark the cross sections for measurement. Survey 2 has an additional cross section, namely CYP8-A, as well as a split CYP0 due to the low water level. The values on the images (c-d) represent suspended sediment concentration (with units of mg/L). The study reach has a length of about 8 km, with some widest cross sections about 3 km wide.

Figure 2. Annual variation of water level and flow discharge at Jiujiang and Hukou stations, and two surveys setup, one in the high flow conditions and the other in the low flow conditions, with a large difference on water level of about 5.8 m. The water level is according to the frozen base level whose zero datum is 1.91 m higher than that of 1985 National Height Datum.

Figure 3. Bed elevations (water level minus water depth) of the confluence (with units of m) before the operation of the Three Gorges Dam in October 2001 (a), and after that in October 2016 (b), and Survey 1 (c) and Survey 2 (d). The contours of 2001 and 2016 were supplied by Bureau of Hydrology and Water Resources of the Lower Reaches of the Yangtze River; and contours of 2018 were calculated by the minus of the water level at Hukou Station and the water depth of the whole study site measured by ADCP. The profiles of the cross sectional bed surface at CYP0 (e), CYP2 (f) and CYP5 (g) are also plotted.

(Note that according to the water level difference between Jiujiang (about 19 km upstream of Hukou), Hukou, Anqing (about 129 km downstream of Hukou), the approximate water surface slope of this reach of the Yangtze River was 0.026‰ (Survey 2) ~ 0.028‰ (Survey 1). That is, the difference of water level between upstream and downstream boundary (totally about 8 km long) was about 21 cm. The water level of the downstream boundary was 15.8 cm lower than that in Hukou, and that of the upstream boundary is 5.2 cm higher than that in Hukou. Comparing to the difference of bed elevation at different time, this difference of water level was neglected. Hence, only the water level at Hukou Hydrological Station was used to represent that of the whole study site).

Figure 4. Sediment concentration at Jiujiang and Hukou hydrological stations before and after the operation of the Three Gorges Dam.

Figure 5. Vectors of vertically-averaged flow velocities of Survey 1 (a) and Survey 2 (b) with units of cm/s.

Figure 6. Difference in depth-averaged velocity magnitude ($\Delta V_{depth\text{-}avg}$; left image) and in flow direction (ΔDir; right image) between Yangtze River and Poyang Lake in two surveys. The horizontal axis shows the distance from the confluence apex near CYP0.

Figure 7. Photos of the mixing interface in Survey 1.

Figure 8. Secondary flows in all cross sections for the case in August Survey 1, looking downstream. (Vector: secondary velocity; contour: primary velocity with units of cm/s)

Figure 9. Raw data of velocity field (left image) and the rotated data by Rozovskii method (right image) at the left side of CYP2 (a), CYP4 (b), and CYP6 (c) in Survey 1, looking downstream. (Vector: secondary velocity; contour: primary velocity with units of cm/s)

Figure 10. Raw data of velocity field (left image) and the rotated data by Rozovskii method (right image) at the right side of CYP2 (a), CYP3 (b), and CYP4 (c) in Survey 1, looking downstream. (Vector: secondary velocity; contour: primary velocity with units of cm/s)

Figure 11. Secondary flows in all cross sections for the case in December Survey 2 (Vector: secondary velocity; contour: primary velocity with units of cm/s).

Figure 12. Grain size distribution of suspended sediment samples taken from the YR, the PL and the confluent zone in Survey 2. Note that 'SS' is suspended load, and 'BM' is bed material. The median grain size, D_{50}, values of bed material in the Yangtze River were 186 μm (I-R), 279 μm (CYP0-L) and 162 μm (left part of CYP1). On the other hand, for the channel out of Poyang Lake, D_{50} at P3 was 20 μm, and at CYP1 (right part) was 17 μm. At the middle of CYP1 where the two flows combine, D_{50} of bed material was 50 μm. D_{50} of suspended load of the Yangtze River and the Poyang Lake were 17 μm and 14 μm, respectively.

Figure 13. Spatial distribution of *RB* (representing suspended sediment concentration) in all cross sections in Survey 1 (Vector: secondary velocity; contour: *RB*).

Figure 14. Spatial distribution of *RB* (representing suspended sediment concentration) in all cross sections in Survey 2 (Vector: secondary velocity; contour: *RB*).

Figure 15. Depth-averaged suspended sediment concentration (represented by *RB*) and depth-averaged flow velocity at the confluence for two surveys.

Table 1.

Main geometric and hydraulic characteristics of the confluence

Characteristic parameters	Survey 1		Survey 2	
	Yangtze River	Poyang Lake	Yangtze River	Poyang Lake
Discharge, Q (m^3/s)	18227	3679	8294	3974
Mean flow velocity, U (m/s)	0.91	0.28	0.86	0.74
Width, W (m)	1930	1562	1133	661
Mean depth, H (m)	10.2	8.5	8.8	7.7
W/H (-)	189	183	129	86
Confluence angle (°)	58		58	
Discharge ratio, Qr (-)	0.2		0.5	
Mean flow velocity ratio, Ur (-)	0.31		0.86	
Flow momentum ratio, Mr (-)	0.06		0.41	

Note: Flow momentum M is calculated by ρQU, where ρ is the water density. The discharge of the Yangtze River excludes that of the branch at the left of the Zhangjia Island.

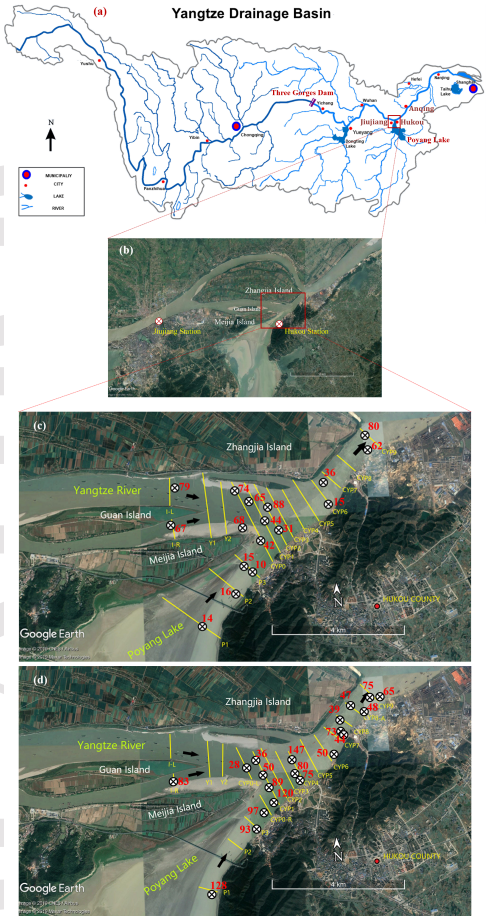

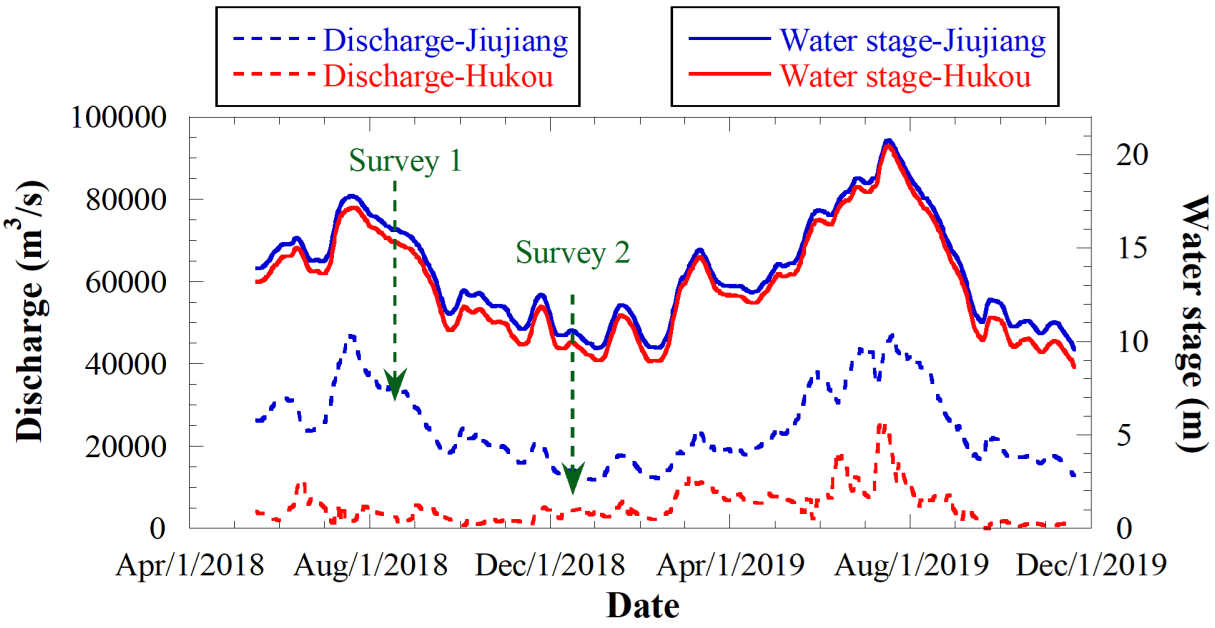

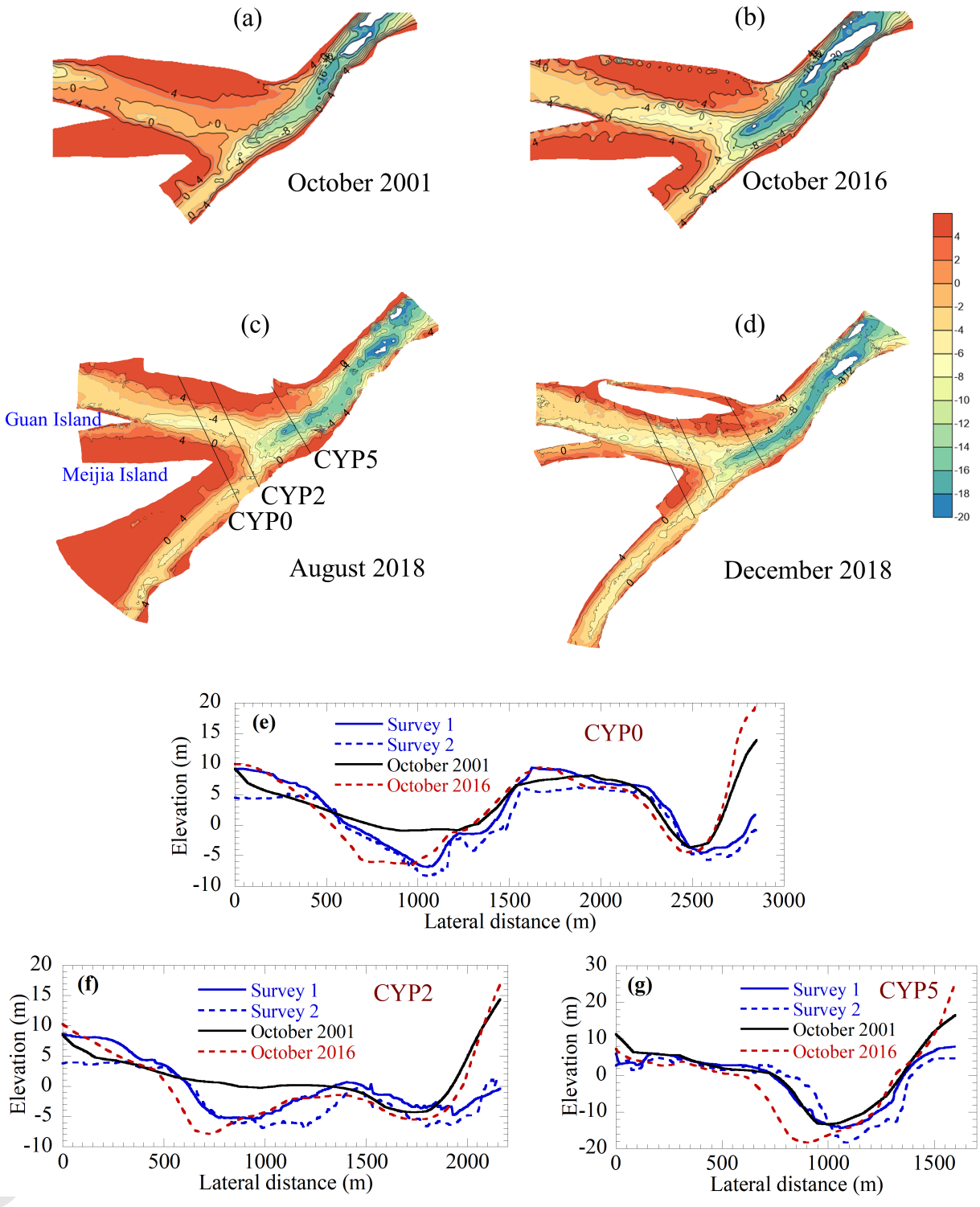

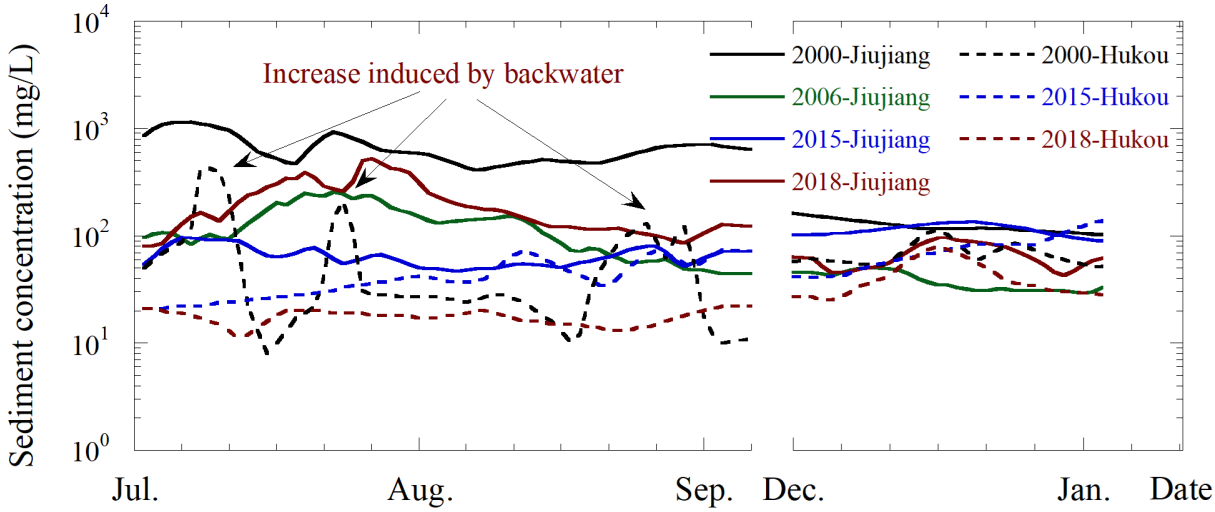

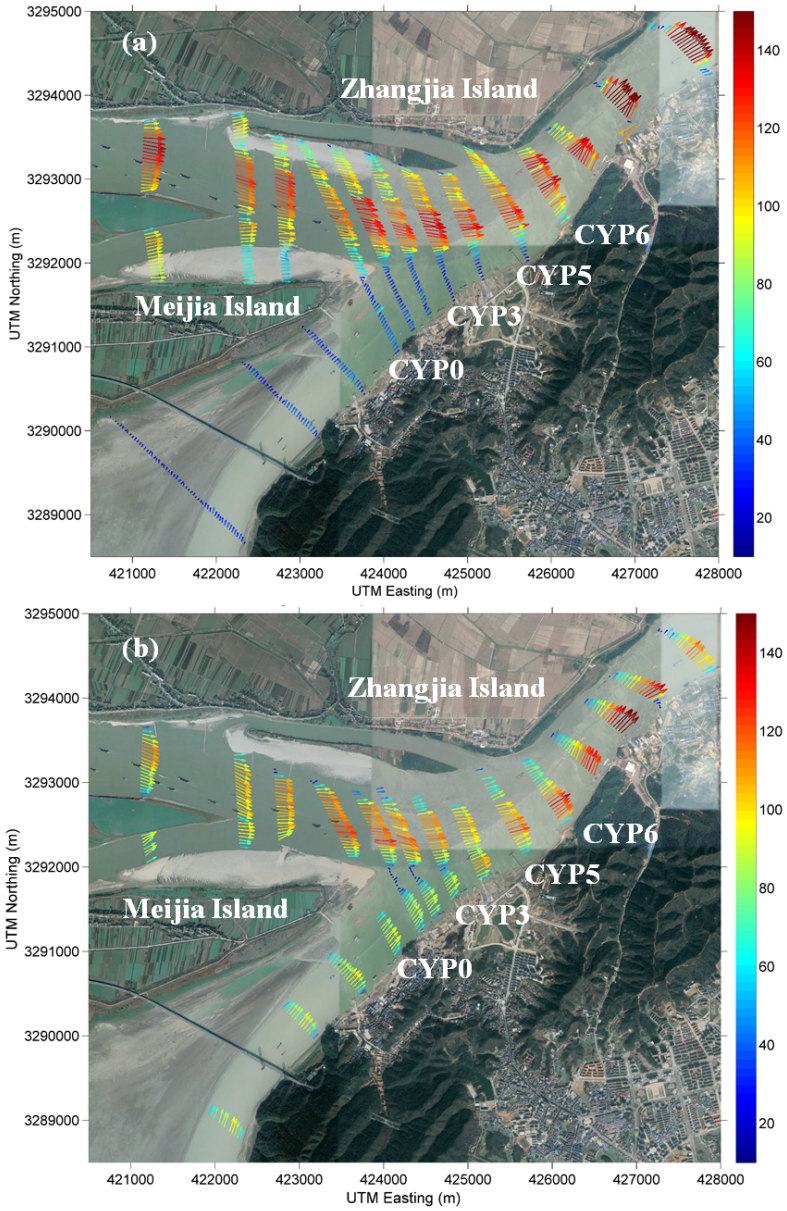

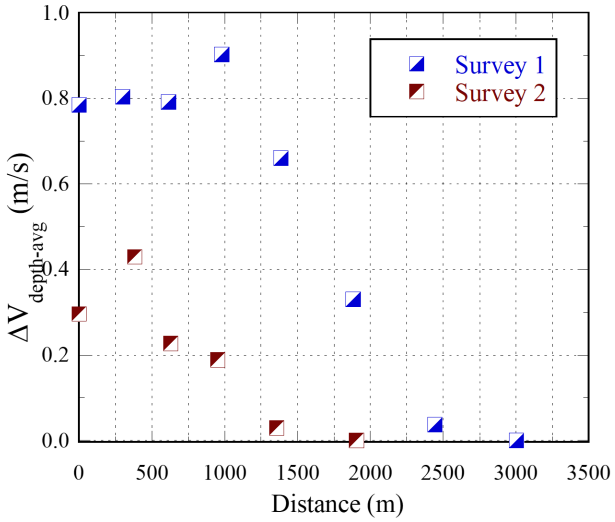

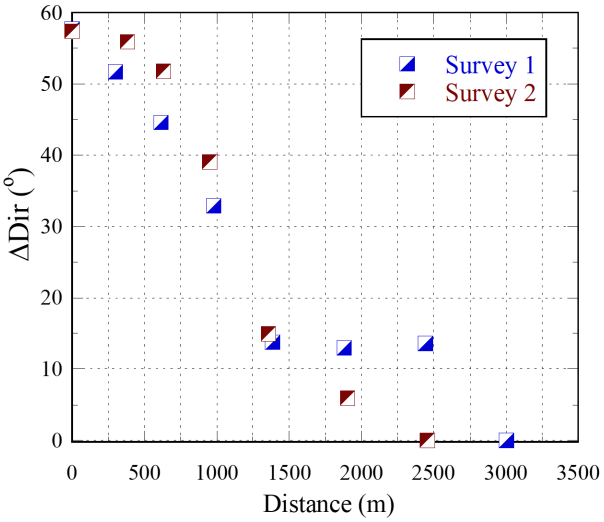

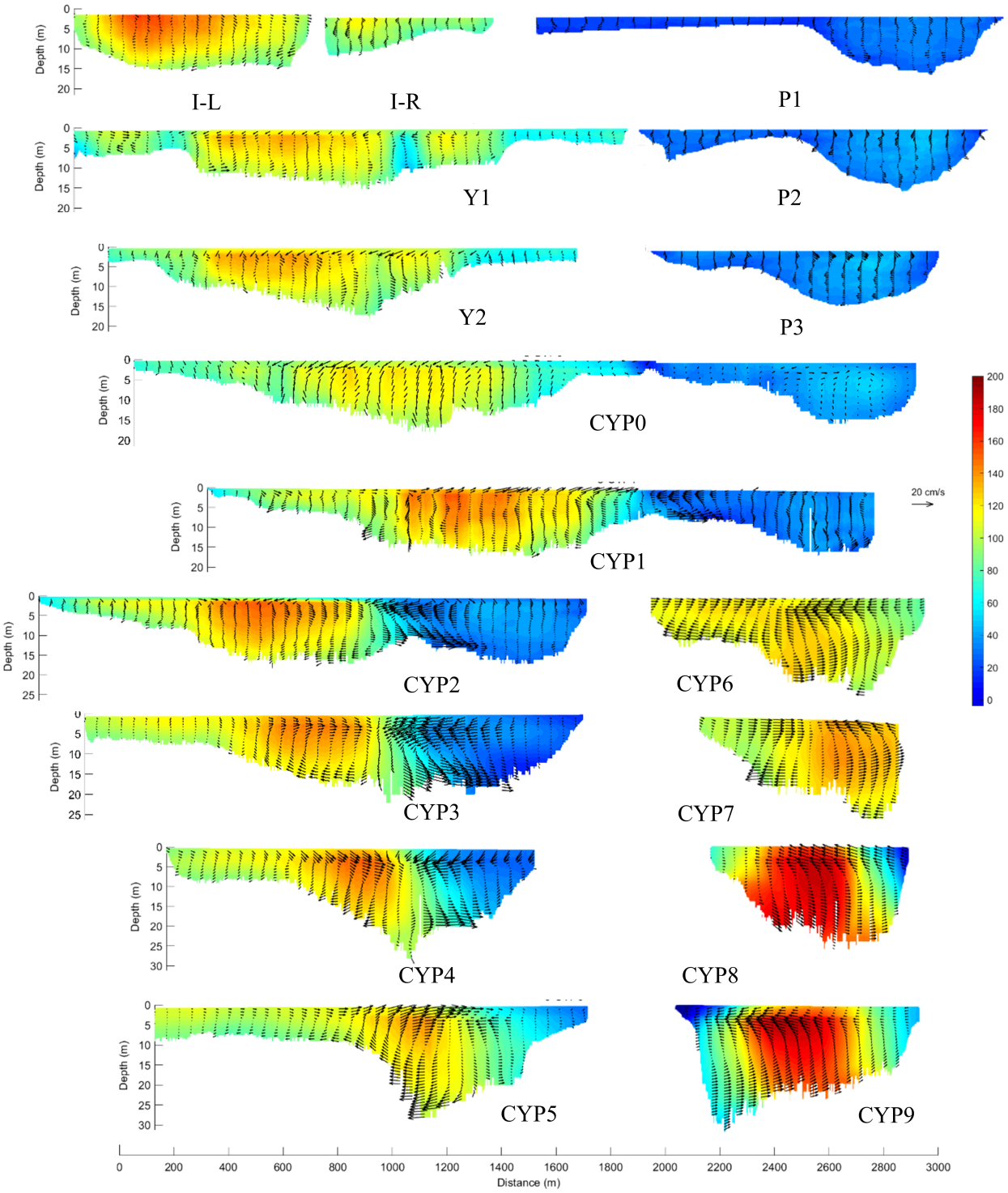

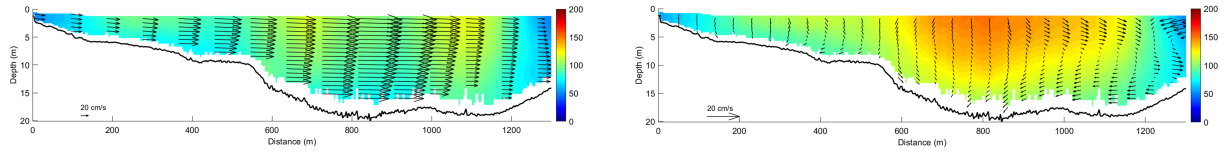

(a) CYP2

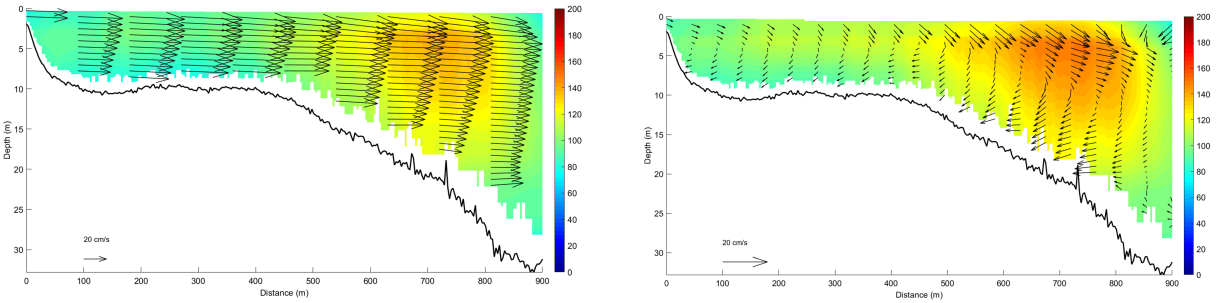

(b) CYP4

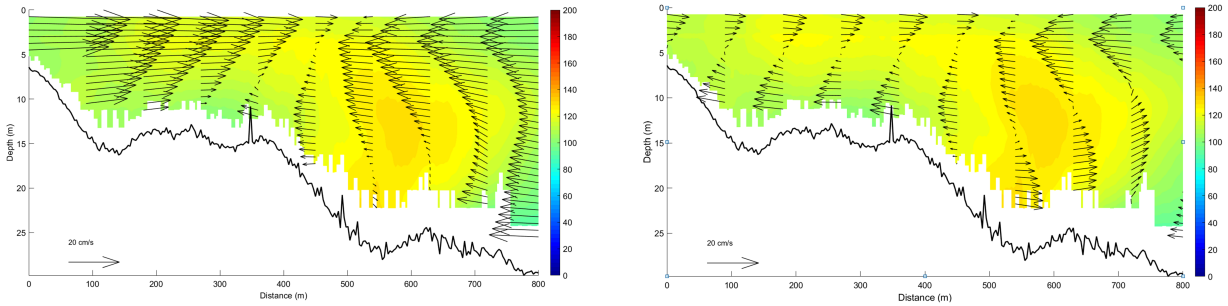

(c) CYP6

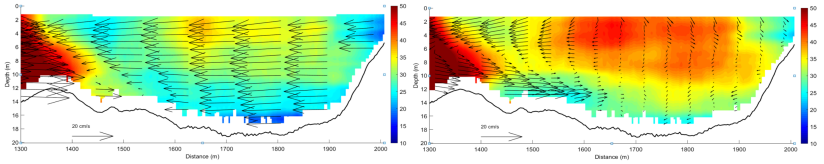

(a) CYP2

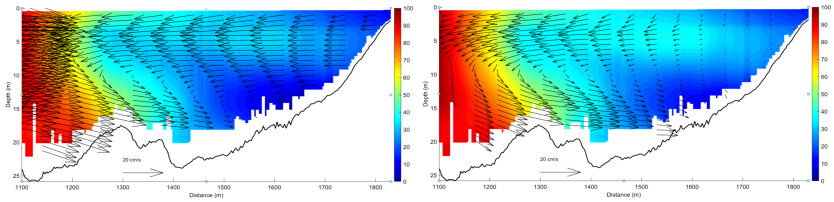

(b) CYP3

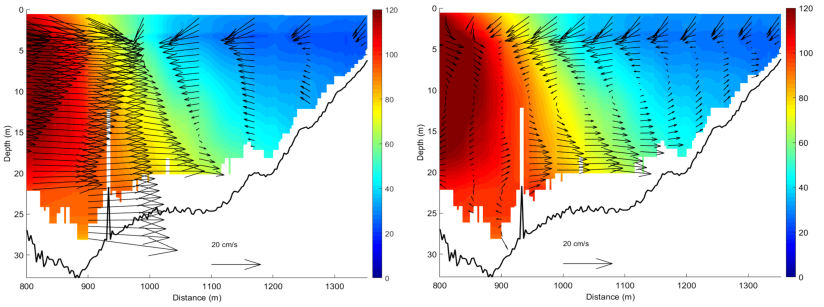

(c) CYP4